Analysis of nuclear spin-lattice relaxation in HCP transition metals based on Dirac theory

1994 J. Phys.: Condens. Matter 6 3965

(http://iopscience.iop.org/0953-8984/6/21/021)

J. Phys.: Condens. Matter 6 (1994) 3965–3986. Printed in the UK

Analysis of nuclear spin–lattice relaxation in HCP transition metals based on Dirac theory

R Markendorf†, C Schober‡ and W John‡

† Physik-Institut, Universität Zürich, Winterthurerstrasse 190, CH-8057 Zürich, Switzerland
‡ Technische Universität Dresden, Institut für Theoretische Physik, D-01062 Dresden, Germany

Received 6 May 1993, in final form 16 February 1994

Abstract. Symmetry adapted expressions for the magnetic and quadrupolar nuclear spin–lattice relaxation time T_1 in HCP metals are derived from Dirac theory. They are applied systematically to 3d, 4d and 5d metals (Sc, Ti, Y, Zr, Tc, Lu, Hf, Re, Os) on the basis of semi-relativistic and full-relativistic self-consistent LMTO calculations. General trends and relativistic effects are discussed. The relaxation rate T_1^{-1} in Zr is overestimated theoretically by a factor of two, as already found by Asada and Terakura. There is strong evidence that the reason for this error lies in spin–orbit splitting. Shifts of 3 mRy in the band position explain the experimental T_1^{-1} in Zr. The Fermi surface of Ti is discussed in connection with the theoretical relaxation rate. Some quantities that are useful for the evaluation of measurements like hyperfine coupling constants and ratios between magnetic and quadrupole relaxation rates are presented. Comparison with the experimental data shows that the quadrupole scattering is well reproduced by the theory.

1. Introduction

In this paper, expressions for magnetic and quadrupole nuclear spin–lattice relaxation by conduction electrons in hexagonal close packed (HCP) metals are derived from Dirac theory. The resulting relations are applied to 3d, 4d and 5d transition metals on the basis of semi- and full-relativistic linear muffin tin orbital (RLMTO) band structure calculations.

After the derivation of a concept capable of describing the relaxation process (Redfield 1955, Hebel and Slichter 1959) and the clarification of the main driving mechanisms (Korringa 1950, Obata 1963, 1964, Yafet and Jaccarino 1964 and Gaspari *et al* 1964), namely Fermi contact, dipole, orbital, electric quadrupole interaction and core polarization, a lot of material-specific estimations of the nuclear spin–lattice relaxation rate T_1^{-1} were made in connection with experiments. Basic inputs were empirical and/or measured electronic structure quantities and atomic data such as hyperfine coupling constants and nuclear moments. One aim was to subdivide the experimental results, which were increasingly detailed with regard to the electronic sources, with the help of estimated atomic constants, s–d-band models and quantities deduced from other experiments. With growing complexity of the electronic structure, this method becomes less reliable and a microscopic treatment is required.

On the basis of fast and accurate band structure calculation methods, which were developed in the 1970s, the extensive experimental material was worked on by many theoreticians in the 1980s. In a series of papers (Asada *et al* 1981, Asada and Terakura 1982, 1983) the nuclear spin–lattice relaxation in pure cubic and HCP metals was examined carefully. The authors of these papers completed the formulae of Narath (1967), who

0953-8984/94/213965+22$19.50

elaborated a part of the magnetic relaxation rate in HCP crystals; they studied 3d and 4d metals (Asada and Terakura 1982, to be referred to hereafter as I) up to a relativistic computation of the contact contribution (Asada and Terakura 1983, to be referred to hereafter as II). A little later John *et al* (1983) presented the complete relativistic formulae for the magnetic and electric quadrupole relaxation rate in cubic metals and applied them to heavier transition metals.

The present work continues the outlined course of investigations for HCP metals. It includes the same metals as I (Sc, Ti, Y, Zr, Tc) and additionally the 4f metal Lu and the 5d metals Hf, Re and Os. Owing to the sensitive dependence of the electronic properties in the nuclear vicinity, relativistic effects influencing T_1^{-1} are already perceptible in lighter metals. This is why we prefer a Dirac description.

A systematic correction is the relativistic contraction of the electronic states near the nuclei, which is most important for the s states (see II). Furthermore, very small band shifts and splittings due to the spin–orbit interaction may change the relaxation rate. These effects on the band structure usually play a minor role for $Z \leqslant 36$ (Akai *et al* 1990), but here we show that very subtle effects on the band structure may have some influence on T_1 in Ti, and alter T_1 appreciably in Zr. A third consequence of the Dirac treatment is the further reduction of the symmetry by spin–orbit coupling, apart from its band effects. In the local HCP point symmetry group D_{3h}, s, p and d states belong to four irreducible representations. Spin–orbit coupled lattice harmonics are invariant under operations of the double-point symmetry group (DPSG) $\mathbf{D}_{3h}$, which has only three irreducible extra representations (Pyykkö and Toivonen 1983). So more different angular momenta l appear in the same representation Γ and interfere in non-diagonal hyperfine scattering terms

$$\langle \Gamma\gamma\kappa_1(l)|H_{\mathrm{hf}}|\Gamma'\gamma'\kappa_1'(l)\rangle\langle\Gamma\gamma\kappa_2(l')|H_{\mathrm{hf}}|\Gamma'\gamma'\kappa_2'(l')\rangle^* \qquad l \neq l'.$$

A further motivation for the studies was the hope of finding reasons for some discrepancies between theory and experiment in I. Beyond that, the extension to 5d metals allows systematic trend investigations and a study of the quadrupole scattering.

In order to examine these points more closely and to improve reliability we thought it advantageous to carry out two series of calculations that include relativistic corrections on different levels. We focus particularly on the question of how relativistic effects and characteristic features of the electronic structure affect T_1.

2. Spin-lattice relaxation rate

In this section, expressions for the practical calculation of the nuclear spin–lattice relaxation by relativistic conduction electrons in HCP metals are introduced. A derivation of these expressions was given by Markendorf (1991). We do not present relativistic formulae for the core polarization, because in this work we use the values from I.

The spin–lattice relaxation in metals is driven by the scattering of electrons at the nucleus. In a T_1 process the hyperfine interaction causes a flip from the nuclear Zeeman state $|m\rangle$ to $|m'\rangle$ and a simultaneous transition between the Bloch states $|k\rangle$ and $|k'\rangle$.

The relaxation rate T_1^{-1} in the spin temperature approximation (Slichter 1990) is

$$\frac{1}{T_1} = \frac{1}{2}\sum_{m,m'} W_{m,m'}(E_m - E_{m'})^2\left(\sum_m E_m^2\right)^{-1} \tag{1}$$

$$W_{m,m'} = \frac{2\pi}{\hbar}\sum_{k,k'}|\langle m'k'|H_{\mathrm{hf}}|mk\rangle|^2 k_{\mathrm{B}}T\delta(E_k - E_{\mathrm{F}})\delta(E_{k'} - E_k). \tag{2}$$

Table 1. Basis functions for the representations of the DPSG $\mathbf{D}_{3h}$. $\Omega^{\Gamma}_{\kappa,\mu}$ are the spin–orbit functions.

Extra representation Γ	Row of Γ γ	Basis functions $\chi^{\Gamma}_{\kappa\gamma}$				
		$l=0$	$l=1$		$l=2$	
Γ_7	1	$\Omega_{-1,1/2}$			$\Omega_{2,1/2}$	$\Omega_{-3,1/2}$
	2	$\Omega_{-1,-1/2}$			$-\Omega_{2,-1/2}$	$\Omega_{-3,-1/2}$
Γ_8	1		$\Omega_{1,1/2}$	$\Omega_{-2,1/2}$		$\Omega_{-3,-5/2}$
	2		$\Omega_{1,-1/2}$	$-\Omega_{-2,-1/2}$		$\Omega_{-3,5/2}$
Γ_9	1			$\Omega_{-2,-3/2}$	$\Omega_{2,3/2}$	$\Omega_{-3,3/2}$
	2			$\Omega_{-2,3/2}$	$\Omega_{2,3/2}$	$-\Omega_{-3,-3/2}$

In equation (1) E_m are the nuclear Zeeman energies and $W_{m,m'}$ is the total transition probability between the Zeeman levels E_m and $E_{m'}$, with E_F being the Fermi energy. These transitions are induced by the hyperfine interactions

$$H_{hf} = H_{mag} + H_q. \tag{3}$$

The Dirac hyperfine operator

$$H_{mag} = \frac{ec\tau\mu_0\hbar\gamma_N \boldsymbol{I}(\boldsymbol{\sigma}\times\hat{\boldsymbol{r}})}{4\pi r^2} \tag{4}$$

describes the magnetic interaction of the electrons with the nuclear dipole moment. It corresponds in the non-relativistic case to the Fermi contact, dipole and orbital interaction. Here τ is the pseudoscalar matrix, γ_N is the nuclear gyromagnetic ratio, $\boldsymbol{I}$ and $\boldsymbol{\sigma}$ are the nuclear and the electron spin operator respectively, e is the electron charge and $\hat{\boldsymbol{r}}$ the unit vector $\boldsymbol{r}/r$ in real space; H_q is the quadrupole interaction

$$H_q = \frac{1}{6}\sum_{i,j} Q_{ij}q_{ij} \tag{5}$$

$$Q_{ij} = \frac{|e|Q}{I(2I-1)}\sum_{i,j}[\tfrac{3}{2}(I_iI_j + I_jI_i) - \delta_{ij}I^2] \tag{6}$$

$$q_{ij} = \frac{e}{4\pi\epsilon_0}\frac{3x_ix_j - r^2\delta_{ij}}{r^5} \tag{7}$$

with the quadrupole tensor Q_{ij}, the quadrupole moment Q and the electronic field gradient operators q_{ij} with the electron coordinates x_i. The transition probabilities (2), (4)–(7) have to be evaluated with the symmetrized Dirac four-component spinors. The relativistic basis functions $\chi^{\Gamma}_{\kappa\gamma}$ for the representations of the DPSG $\mathbf{D}_{3h}$ are presented in table 1 (Pyykkö and Toivonen 1983). According to the interactions T_1^{-1} has two parts:

$$\left(\frac{1}{T_1}\right) = \left(\frac{1}{T_1}\right)_{mag} + \left(\frac{1}{T_1}\right)_q. \tag{8}$$

In the resulting formulae the hyperfine coupling constants occur, which we defined as

$$H_{\kappa\kappa'} = \mu_B\frac{\mu_0}{4\pi}\frac{2m_0c}{\hbar}\int_0^{r_{WS}}(g_\kappa f_{\kappa'} + g_{\kappa'}f_\kappa)\,dr \tag{9}$$

$$q_{\kappa\kappa'} = \left(\frac{3(2I+3)}{10I^2(2I-1)}\right)^{1/2}\int_0^{r_{WS}}(g_\kappa g_{\kappa'} + f_{\kappa'}f_\kappa)\frac{dr}{r} \tag{10}$$

and the quantities

$$n^{\Gamma}_{\kappa\kappa'} = n^{\Gamma}_{\kappa\kappa'}(E_F) = \sum_k c^*_{\Gamma\gamma\kappa}(k) c_{\Gamma\gamma\kappa'}(k) \delta(E_k - E_F) \tag{11}$$

which are in the diagonal case $\kappa = \kappa'$ the partial density of states (DOS) of κ orbitals of the representation Γ and in the non-diagonal case the so-called mixed (or off-diagonal) DOS. The hyperfine couplings $H_{\kappa\kappa}$ are related to H_F and H^l_{orb} in I via equations (14)–(16). The quantities $c_{\Gamma\gamma\kappa}$ are expansion coefficients of the Bloch states and g_κ and f_κ are the radial parts of the major and the minor component in the Dirac spinor at the Fermi energy. The integrals reach out to the Wigner–Seitz radius r_{WS}. The explicit formulae for the two contributions in (8) are given in the appendix.

The magnetic and quadrupole operators (4), (6), (7) do not interfere in the scattering rates because their tensor components transform with respect to rotation matrices of the first and the second rank, respectively. Our relaxation rates are labelled as the corresponding terms in I. The magnetic terms have to be assigned to the sum of the dipolar and orbital terms and, for s states, to the Fermi contact contribution. So far we have carried out the non-relativistic symmetry-adapted limits for $(T_1^{-1})^{p}_{mag}$, $(T_1^{-1})^{s-d}_{mag}$, $(T_1^{-1})^{p}_{q}$ and $(T_1^{-1})^{d}_{q}$ and have arrived with the corresponding formulae in I. (The last line of equation (14) in I contains a misprint: E'' in the term $-8n_{A'd}n_{E''d}$ must be replaced by E'.)

3. Practical calculations and approximations

This section describes the calculation of the electronic structure and the approximations used in applying the foregoing formulae inclusive of the appendix.

All calculations rest on self-consistent band structure work with the LMTO and RLMTO method (Andersen 1975). For each 3d and 4d metal we performed two independent band structure calculations. Relativistic effects are considered on the one hand within the scope of the scalar-relativistic LMTO version (Skriver 1984), which contains the mass–velocity and Darwin corrections up to any order using a method related to Koelling and Harmon (1977). On the other hand, the second series of RLMTO calculations is also derived from the Skriver computer code and is directly based on Dirac theory (Eriksson 1989).

The following specifications refer to both methods. They start with renormalized relativistic atomic charge densities. In the atomic and band structure calculations the exchange and correlation potential of von Barth and Hedin (1972) was used. The lattice sum in the structure constants was extended over about 30 atomic shells in direct space as well as in reciprocal space, so that their numerical error is lower than 0.1%. The underlying c/a ratios listed in table 2 are experimental values (Wyckoff 1974). In each iteration the band structure data at 64 k-points in the irreducible part of the Brillouin zone (IBZ) and in the final two iterations at 448 k-points in the IBZ were used to construct the new potential. The partial DOS were obtained by the tetrahedron method (Jepsen and Andersen 1971, Lehmann and Taut 1972). To all materials the complete LMTO formalism including the combined muffin tin corrections was applied. The basis set includes s, p and d states leading in the RLMTO scheme to an eigenvalue problem of the dimension 36×36. Concerning the calculation of the relaxation rate, we have to distinguish between two series.

(i) *Series 1.* The T_1T values, resting on scalar-relativistic band structures are named series 1. In this case we proceed as follows. After achieving self-consistency, the Dirac equation is integrated in the crystal potential at the Fermi energy. The so-determined radial parts of the major and minor components show practically no difference to the strict

Table 2. Lattice constants in Bohr radii, partial DOS in states per spin orbital atom Ry and hyperfine coupling constants in 10^2 T (10^6 Oe in I). The results belong to series 2 for 3d and 4d metals and to series 1 for 5d metals.

	Sc	Ti	Y	Zr	Tc	Lu	Hf	Re	Os
a	6.251	5.575	6.888	6.104	5.168	6.620	6.038	5.216	5.168
c/a	1.592	1.586	1.572	1.593	1.604	1.585	1.583	1.612	1.579
n_{-1-1}	0.198	0.064	0.251	0.085	0.101	0.075	0.044	0.056	0.024
n_{11}	1.279	0.359	1.167	0.469	0.265	1.544	0.395	0.231	0.074
n_{-2-2}	1.251	0.353	1.132	0.519	0.247	1.544	0.395	0.231	0.074
n_{22}	1.984	1.031	1.799	1.121	0.837	1.543	0.710	0.764	0.765
n_{-3-3}	1.967	0.974	1.719	0.872	1.004	1.543	0.710	0.764	0.765
H_{-1-1}	−4.272	−5.843	−8.100	−11.170	−17.218	−23.784	−30.853	−46.531	−52.242
H_{11}	1.277	1.857	2.648	3.878	5.863	6.886	9.574	14.633	15.408
H_{-2-2}	−0.620	−0.901	−1.245	−1.820	−2.717	−2.661	−3.679	−5.389	−5.418
H_{22}	0.391	0.649	0.490	0.845	2.089	1.047	1.666	3.649	4.943
H_{-3-3}	−0.254	−0.424	−0.311	−0.536	−1.312	−0.588	−0.934	−2.000	−2.698
H_s	2.848	3.896	5.400	7.447	11.478	15.857	20.569	31.021	34.828
H_p	0.626	0.910	1.271	1.860	2.788	2.922	4.048	6.031	6.180
H_d	0.128	0.214	0.159	0.274	0.672	0.316	0.502	1.087	1.468

relativistic results. Since there is no distinction between different total angular momenta, all $n^{\Gamma}_{\kappa\kappa}$ with $\kappa = l$ or $\kappa = -l-1$ are approximated by the same value:

$$n^{\Gamma}_{\kappa\kappa} = \frac{N_l}{2(2l+1)} \tag{12}$$

where N_l is the partial number of l states per Ry and atom. The mixed DOS and hyperfine coupling constants are handled similarly in the series of Dirac calculations. Series 1 contains all metals under consideration.

(ii) *Series 2.* The calculations in the framework of Dirac theory are called series 2. Since we did not subdivide the DOS of the κ states with regard to the representations Γ any further, we assume that every representation $\Gamma(\kappa)$ enters the partial κ-DOS with the same weight:

$$n^{\Gamma}_{\kappa\kappa} = \frac{N_\kappa}{2|\kappa|} \tag{13}$$

where N_κ is the partial density of κ orbitals in states per Ry and atom. So the densities $n^{\Gamma_7}_{-1-1}$ and $n^{\Gamma_8}_{11}$ are in the T_1 calculation exactly. Table 2 shows the partial DOS of this series for 3d and 4d metals, and of series 1 for 5d metals. The mixed DOS $|n^{\Gamma}_{\kappa\kappa'}|^2$ are approached by $n^{\Gamma}_{\kappa\kappa}n^{\Gamma}_{\kappa'\kappa'}/2$, which is only an empirical value. This is of course the poorest approach made here. The amounts of the actual mixed DOS may deviate considerably from it. All terms in equations (A3)–(A14), which contain real parts of a DOS product, have been neglected because they are not fixed in sign and the real parts of the expansion coefficient products compensate partly in the summation at an isoenergy surface. This also shows up in the non-relativistic limit, where all these DOS lead to *differences* between two densities, except for the s–d and p–d mixed DOS. For example, the density $n^{\Gamma_7}_{2-3}$ is in the non-relativistic transition equal to $\sqrt{6}/5(n_{E''\mathrm{d}} - n_{A'\mathrm{d}})$. Due to the local character of T_1^{-1} the radial integrals are, with good accuracy, restricted to the WS sphere (Asada *et al* 1981, Akai 1988), as already

involved in the formulae of the preceding section. Series 2 contains only the 3d and 4d metals.

In summation, both computation series use the correct Dirac hyperfine interaction. The essential difference is that in series 1 the consequences of spin–orbit coupling for the band behaviour at the Fermi energy and therefore in the DOS are disregarded.

Contributions due to matrix elements (A15) with different angular momenta have been checked. The s–d term H_{-12} is, for example, three orders of magnitude smaller than the s term H_{-1-1}. If all such terms, which were omitted in the formulae in the appendix, are included, they contribute $2 \times 10^{-4}\%$ to the magnetic relaxation and $5 \times 10^{-4}\%$ to the quadrupole relaxation in Sc.

Often the non-relativistic coupling constants are of interest for practical estimations. The following combinations of the $H_{\kappa\kappa}$ yield the usual coupling constants in the non-relativistic limit:

$$H_s = -\tfrac{2}{3}H_{-1-1} \tag{14}$$

$$H_\pm^l = \frac{H_{\kappa\kappa}}{\kappa + 1} \qquad \kappa = \begin{cases} l \\ -l-1. \end{cases} \tag{15}$$

For non-s terms we define one uniform coupling constant for a given l:

$$H_l = \frac{l H_+^l + (l+1)H_-^l}{2l+1}. \tag{16}$$

The terms H_s and H_l are the relativistic counterparts of the Fermi contact coupling H_F and H_{orb}^l in I, respectively. All these coupling constants are listed in table 2, because they are useful for the further analysis of measured data. The combinations (16) agree excellently for all metals with H_{orb}^l in I.

4. Results and discussion

This section gives a survey of the final results, which are subsequently discussed in view of the focal aspects.

4.1. Survey of results and general trends

The metals in question permit systematic investigations, because some of them have equal valences and therefore similar electronic structure. The main quantities that affect the relaxation rate are the hyperfine coupling constants and the partial DOS.

The hyperfine coupling constants are shown in figure 1. To compress the data, we use the combination (16) of the two hyperfine constants corresponding to angular momentum l. The quantity H_l does not enter T_1^{-1} directly, but is suitable to give a qualitative survey of trends, and it has the advantage of providing the usual coupling constants in the non-relativistic limit. Figure 1 was restricted to p and d states, since they determine T_1^{-1} in transition metals. The constants H_p and H_d increase from the 3d to the 4d period within one group by factors of about 2 and 1.3, and from the 4d to the 5d period by about 2.4 and 1.9, respectively. Along a period, H_d increases more strongly than H_p for reasons of different local character of p and d states (Asada and Terakura 1981).

The increase of the hyperfine coupling in one group is contrasted by the decrease of the DOS at the Fermi energy. To simplify matters, figure 2 shows only the total DOS. It shows

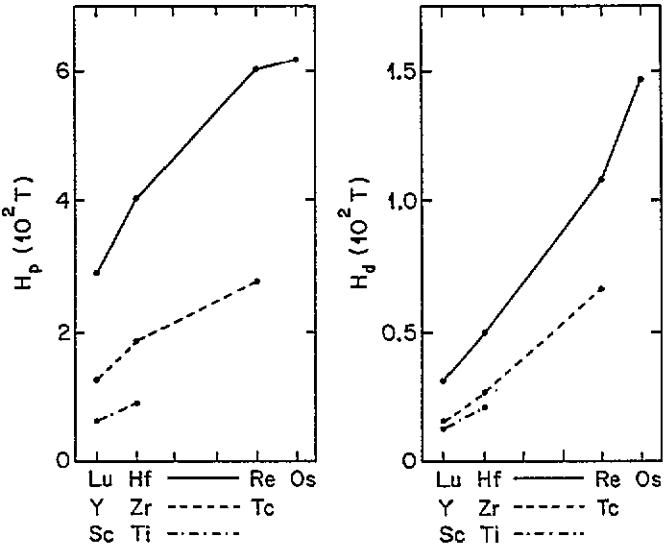

Figure 1. Relativistic magnetic hyperfine coupling constants H_p and H_d for p and d states at the Fermi energy.

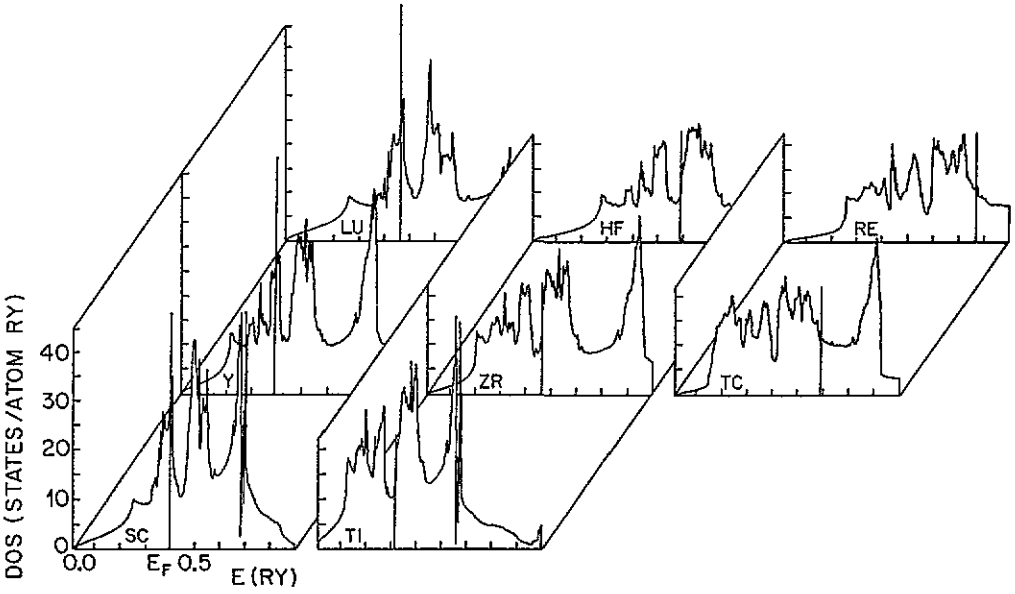

Figure 2. Total DOS for HCP metals in a uniform scale, calculated by the complete self-consistent LMTO method.

that the d bands get broader from 3d to 5d metals due to the overlap of the d valence states. Further element-specific features of the DOS are given in section 4.2.

The total magnetic relaxation rate, divided by the squared gyromagnetic ratio $(\mu/I)^2$, shows that the increase of the hyperfine coupling is the decisive tendency from one period to the next, which is only slightly diminished by the band broadening (see figure 3). The

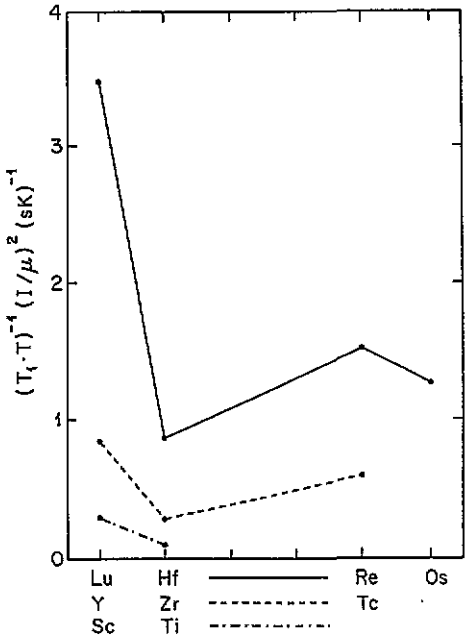

Figure 3. Theoretical magnetic relaxation rates $(T_1T)^{-1}_{mag}$ divided by $\gamma_N^2 = (\mu/I)^2$, with μ in nuclear magnetons and I in units of $\hbar$.

alteration of the DOS at the Fermi energy recurs systematically in every period, a fact that also shows up in the relaxation rate.

Tables 3 and 4 show the results of series 1, i.e. founded on the scalar-relativistic LMTO scheme with relativistically correct hyperfine coupling, and table 5 shows the results of the full Dirac calculations of series 2. The contribution of the core polarization $(T_1T)^{-1}_{cp}$ and the final results $(T_1T)^{-1}_{Asada}$ are taken from I and II respectively. The measurements $(T_1T)^{-1}_{exp}$ were reviewed by Carter *et al* (1977), with the exception of Zr (Hioki *et al* 1975, I) and Re (Dimitropoulos *et al* 1989). The very small p–d quadrupole contributions (A14) have been omitted in all these tables. $(T_1T)^{-1}_{total\ poly}$ is the rate averaged over all directions, i.e. for $\sin^2\beta = 2/3$. The quadrupole moment of ^{91}Zr has been found in Büttgenbach *et al* (1978), enabling us to include its quadrupole relaxation in addition to I and II.

At the beginning of the d series, relaxation by p states may compete with that of d states because of the stronger electron–nucleus coupling of p states. This is seen in other quantities of local character, for example the field gradient examinations of Blaha *et al* (1988). The tables make it clear that the relative proportion of p relaxation increases in metals with equal valences, for example from Sc to Lu, because the p coupling is visible enhanced more strongly than the d coupling. This leads to the fact that, in the 5d metals, p relaxation is relatively large up to Re in the middle of the period.

In the 5d series only measurements in Re by Dimitropoulos *et al* (1989) were available. The measured T_1 agrees fairly well with the numerical value, whereas the partition of the total relaxation rate into s and d contributions deviates from theory. Using an s–d two-band model, Dimitropoulos found the magnetic contributions $(T_1T)^{-1}_s = 1.48$ and $(T_1T)^{-1}_d = 1.15$, whilst our diagonal magnetic results for ^{185}Re are $(T_1T)^{-1}_s = 0.42$, $(T_1T)^{-1}_p = 0.78$ and $(T_1T)^{-1}_d = 1.11$ in units of $(sK)^{-1}$. The main reasons for the

Table 3. Theoretical relaxation rates $(T_1T)^{-1}$ in s^{-1} K^{-1} for 3d and 4d metals, series 1. A pair of numbers $a(b)$ means $a + b\sin^2\beta$. For $(T_1T)^{-1}_{cp}$, $(T_1T)^{-1}_{Asada}$ and $(T_1T)^{-1}_{exp}$ see text.

	^{45}Sc	^{47}Ti	^{49}Ti	^{89}Y	^{91}Zr	^{99}Tc
Diagonal						
CP	0.056	0.0007	0.0007	0.0062	0.0060	0.033
s mag	*0.009*	*0.0006*	*0.0006*	*0.0145*	*0.0038*	*0.175*
$p_{1/2}$ mag	0.293	0.0017	0.0017	0.0297	0.0350	0.133
$p_{3/2}$ mag	0.110	0.0006	0.0006	0.0105	0.0124	0.046
$p_{1/2}$ $p_{3/2}$ mag	−0.096(0.085)	−0.0006(0.0005)	−0.0006(0.0005)	−0.0096(0.0084)	−0.0113(0.0099)	−0.042(0.037)
$d_{3/2}$ mag	0.069	0.0034	0.0034	0.0043	0.0127	0.372
$d_{5/2}$ mag	0.042	0.0024	0.0024	0.0025	0.0074	0.212
$d_{3/2}$ $d_{5/2}$ mag	−0.015(0.023)	−0.0008(0.0012)	−0.0008(0.0012)	−0.0009(0.0014)	−0.0027(0.0041)	−0.079(0.120)
$p_{3/2}$ quad	*0.0002*	*0.0001*	0.	——	0.0004	0.0001
$p_{1/2}$ $p_{3/2}$ quad	0.0004	0.0002	0.0001	——	0.0007	0.0002
$d_{3/2}$ quad	0.	0.0001	0.	——	0.	0.0001
$d_{5/2}$ quad	0.	0.0001	0.	——	0.0001	0.0001
$d_{3/2}$ $d_{5/2}$ quad	0.	0.	0.	——	0.	0.0001
Non-diagonal						
s d mag	*−0.006(0.009)*	*−0.0003(0.0005)*	*−0.0003(0.0005)*	*−0.0019(0.0027)*	*−0.0017(0.0024)*	*−0.064(0.088)*
p d mag	0.(−0.112)	0.(−0.0020)	0.(−0.0020)	0.(−0.0085)	0.(−0.0160)	0.(−0.167)
Total poly	0.467	0.0084	0.0081	0.0578	0.0630	0.838
Asada	0.450	0.00708	0.0067	0.0548	0.0665	1.069
Experiment	*0.77 ± 0.23*	*0.0067 ± 0.0013*	*0.0067 ± 0.0013*	*0.067 ± 0.0010*	*0.035 ± 0.005*	*1.25 ± 0.25*

Table 4. As table 3 for 5d metals, series 1.

	^{175}Lu	^{176}Lu	^{177}Hf	^{179}Hf	^{185}Re	^{187}Re	^{187}Os	^{189}Os
Diagonal								
s mag	0.05	0.03	0.002	0.0008	0.42	0.42	0.0010	0.011
$p_{1/2}$ mag	1.76	0.90	0.016	0.006	0.71	0.72	0.0008	0.009
$p_{3/2}$ mag	0.42	0.21	0.004	0.002	0.15	0.16	0.0002	0.002
$p_{1/2}$ $p_{3/2}$ mag	−0.49(0.41)	−0.25(0.21)	−0.005(0.004)	−0.002(0.002)	−0.19(0.16)	−0.19(0.16)	−0.0002(0.0002)	−0.002(0.002)
$d_{3/2}$ mag	0.06	0.03	0.003	0.001	0.77	0.79	0.0132	0.153
$d_{5/2}$ mag	0.03	0.02	0.001	0.0004	0.33	0.34	0.0056	0.065
$d_{3/2}$ $d_{5/2}$ mag	−0.01(0.02)	−0.01(0.01)	−0.0005(0.0007)	−0.0002(0.0003)	−0.14(0.22)	−0.15(0.22)	−0.0025(0.0037)	−0.028(0.043)
$p_{3/2}$ quad	2.77	1.11	0.100	0.054	0.14	0.13	——	0.005
$p_{1/2}$ $p_{3/2}$ quad	6.25	2.50	0.225	0.002	0.33	0.31	——	0.013
$d_{3/2}$ quad	0.05	0.02	0.007	0.004	0.08	0.08	——	0.050
$d_{5/2}$ quad	0.05	0.02	0.008	0.004	0.08	0.07	——	0.047
$d_{3/2}$ $d_{5/2}$quad	0.03(0.005)	0.01(0.002)	0.004(0.0007)	0.188(0.0004)	0.05(0.008)	0.04(0.007)	——	0.028
Non-diagonal								
s d mag	−0.02(0.02)	−0.008(0.01)	−0.0007(0.0008)	−0.0003(0.0003)	−0.17(0.21)	−0.17(0.21)	−0.0011(0.0013)	−0.013(0.015)
p d mag	0(−0.21)	0.(−0.11)	0.(−0.004)	0.(−0.002)	0.(−0.45)	0.(−0.45)	0.(−0.0019)	0.(−0.022)
Total poly	11.10	4.66	0.366	0.196	2.65	2.64	0.0192	0.369
Experiment	——	——			2.63	2.63		

Table 5. As table 3 for 3d and 4d metals, series 2.

	^{45}Sc	^{47}Ti	^{49}Ti	^{89}Y	^{91}Zr	^{99}Tc
Diagonal						
CP	0.056	0.0007	0.0007	0.0062	0.0060	0.033
s mag	0.051	0.0005	0.0005	0.0122	0.0096	0.186
$p_{1/2}$ mag	0.193	0.0017	0.0017	0.0281	0.0350	0.150
$p_{3/2}$ mag	0.069	0.0006	0.0006	0.0093	0.0151	0.044
$p_{1/2}$ $p_{3/2}$ mag	−0.062(0.055)	−0.0006(0.0005)	−0.0006(0.0005)	−0.0087(0.077)	−0.0124(0.0109)	−0.045(0.039)
$d_{3/2}$ mag	0.069	0.0028	0.0028	0.0037	0.0152	0.304
$d_{5/2}$ mag	0.042	0.0015	0.0015	0.0019	0.0054	0.249
$d_{3/2}$ $d_{5/2}$ mag	−0.051(0.023)	−0.0006(0.0009)	−0.0006(0.0009)	−0.0008(0.0011)	−0.0025(0.0039)	−0.078(0.118)
$p_{3/2}$ quad	0.0001	0.0001	0.	——	0.0004	0.0001
$p_{1/2}$ $p_{3/2}$ quad	0.0003	0.0002	0.0001	——	0.0008	0.0002
$d_{3/2}$ quad	0.	0.	0.	——	0.	0.0001
$d_{5/2}$ quad	*0.*	*0.0001*	*0.*	——	*0.*	*0.0002*
$d_{3/2}$ $d_{5/2}$ quad	0.	0.	0.	——	0.	0.0001
Non-diagonal						
s d mag	−0.014(0.020)	−0.0003(0.0004)	−0.0003(0.0004)	−0.0018(0.0023)	−0.0040(0.0045)	−0.041(0.076)
p d mag	0.(−0.090)	0.(−0.0017)	0.(−0.0017)	0.(−0.0073)	0.(−0.0016)	0.(−0.174)
Total poly	0.397	0.0070	0.0067	0.0526	0.0708	0.844
Asada	0.450	0.00708	0.0067	0.0548	0.0665	1.069
Experiment	0.77 ± 0.23	0.0067 ± 0.0013	0.0067 ± 0.0013	0.067 ± 0.0010	0.035 ± 0.005	1.25 ± 0.25

overestimation of the s contribution by the experimental analysis lie in the hyperfine coupling and the model. The $H_{d,Dimi}$ value used ($H_{d,Dimi} = 0.7 \times 10^2$ T (10^6 G)), as estimated by Dimitropoulos from the free-atom $\langle r^{-3} \rangle$ value, is too low because enhancement rather than reduction should be used, as was stated by Asada *et al* (1981), referring to the renormalized atomic picture of Hodges *et al* (1972). In addition, relativistic effects enhance H_d, particularly in the 5d series. We found for a d state at the Fermi energy in Re $H_d = 1.1 \times 10^2$ T. Furthermore, the p states cannot be neglected because in comparison with d states they increase in importance the higher the period number is. That is why the calculated relaxation rate by p electrons of magnetic plus quadrupolar origin is even larger than the rate of d electrons.

Table 6. Comparison of relativistic corrections for s hyperfine coupling from band structure C_s with Pyykkö $C_{s,Py}$.

	C_s	$C_{s,Py}$
Sc	1.048	1.051
Ti	1.056	1.056
Y	1.183	1.192
Zr	1.156	1.203
Tc	1.181	1.241

Pyykkö *et al* (1973) calculated the relativistic correction factors for magnetic hyperfine interactions with hydrogen-like atomic functions analytically, and tabulated them for the outermost s, $p_{1/2}$ and $p_{3/2}$ states up to $Z = 100$. In table 6 we compare the Pyykkö correction $C_{s,Py}$ for s states with the quotient

$$C_s = \frac{H_s}{H_F} \tag{17}$$

from band structure, as has already been done in II. The good agreement between C_s and $C_{s,Py}$ for 3d metals is due to the nearly Coulombic potential in the closer nuclear environment, which is significant for the s coupling (apart from the differences between the atomic and Fermi energies). In the 4d metals the slightly increased screening in this region causes slightly larger differences.

4.2. Relativistic band effects

We now discuss band effects, which influence the number of electrons relaxing the nuclei.

We deal with the elements Ti and Zr, which have four valence electrons. Both metals supply a good background as to the experimental and theoretical material. Jepsen examined the similarity of the electronic structures, in particular the Fermi surfaces of Ti (Jepsen 1975) and Zr, Hf (Jepsen *et al* 1975). According to Jepsen the third, nearly unoccupied, band in Ti at the ΓA line of the IBZ additionally intersects the Fermi energy (see figure 4) causing a change in the topology of the Fermi surface in comparison with 4d and 5d metals of the same column in the periodic table (Zr, Hf). Jepsen *et al* (1975) guessed that in Zr the band in question takes the same turn. Our theoretical T_1^{-1} values and energy bands in series 1 and 2 are useful for evaluating these statements.

Figure 4 contrasts the scalar-relativistic bands of Ti near the Fermi energy with the full relativistic ones. In figure 4(*a*), and in the work of Jepsen, which includes relativistic effects according to Andersen (1975), the hole Fermi surface parts Γ3h and A3h are disconnected.

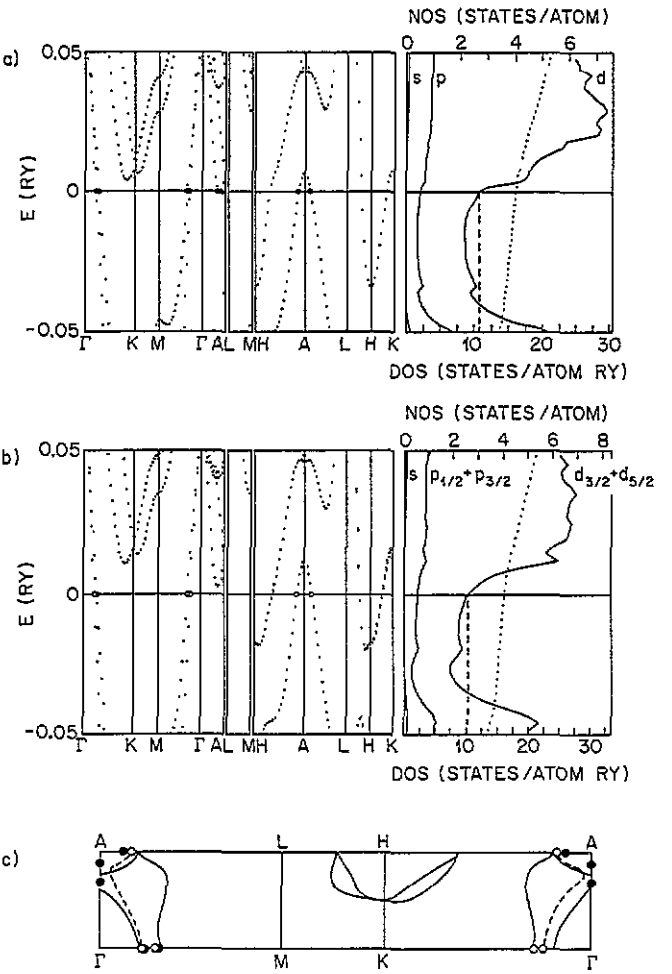

Figure 4. Cut of (*a*) scalar-relativistic and (*b*) relativistic band structure for Ti near the Fermi energy. In (*c*) we compare the sections of the Fermi surface parts Γ3h and A3h in the symmetry planes according to Jepsen (1975) (full curves) with (*a*) (full circles) and (*b*) (open circles, broken curve).

Here the first symbol (or the first two symbols in the case of an open surface) denote(s) the centre of the surface (or the open direction), followed by the number of the band in which it lies; h stands for the hole character. In non-relativistic calculations with the optimized LCAO method, developed by Eschrig, the third band dips more distinctly, namely by about 7 mRy, into the occupied region (Eschrig 1988). In our calculations this band has, in the occupied part along the ΓA line near A, 65%d, 32%p and 3%s character, with increasing d character up to 82% at the point A. In both relativistic calculations of figure 4 this band is shifted up with respect to the Fermi energy, compared with Eschrig, because the d states are lowered less than s and p states by relativistic effects. The band considered is, in the region of intersection, further shifted by 3 mRy in the Dirac calculation (figure 4(*b*) against figure 4(*a*)) and steps out of the occupied conduction band. So the two closed hole surfaces Γ3h, A3h connect to a surface ΓA3h opened along the line Γ*A*. To get some evidence regarding the actual location of this band we exploit the strong dependence of T_1^{-1} upon

the partial DOS. By the stepping out of the discussed band, the DOS decreases by about one state per Ry per atom. Heeding the above-mentioned portions of l character it is clear that this concerns mostly the d states. Fortunately, the d states supply the dominant contribution to T_1^{-1} in Ti and therefore the very subtle band shift influences are discernible only in the Ti d relaxation rate in tables 3 and 5. The results of series 2 approach the measured values very well (see table 5). Hence a comparison of the two series with experiment hints that the Fermi surface of Ti contains an open ΓA3h surface part and is topologically equivalent to that of Zr and Hf. Nevertheless, this discussion has only an exemplary character for similar cases. The differences in the rates are too small for a clear decision.

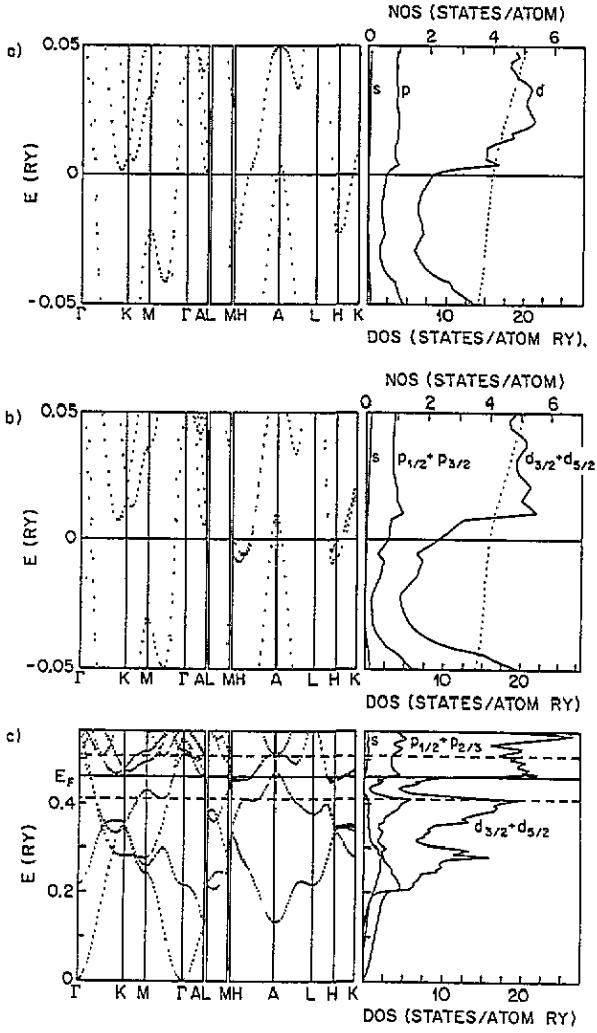

Figure 5. Stretched cut of the (*a*) scalar-relativistic and (*b*) relativistic band structure for Zr near the Fermi energy. In (*c*) we show the whole occupied region of the Dirac band structure, containing the cut *b*) between the broken lines.

The corresponding band structure cuts for Zr are shown in figure 5. The band in discussion lies fully in the unoccupied region in the scalar-relativistic version of series 1

along ΓA. The Fermi surface has a similar form to the ΓA3h hole surface of figure 4. Jepsen *et al* (1975) register d bands somewhat too low lying in comparison with measured electronic heat capacities and with de Haas–van Alphen measurements (Everett 1972a, b), suggesting a relative upward shift of the d bands by about 10–20 mRy in Zr. Though we cannot support the dissection of the ΓA3h hole surface proposed by them, we see the same general trend of the d states in our self-consistent calculations, namely that agreement with experiment would require a raising of the d bands against the Fermi energy by about 3 mRy. A hint about the relative shift of the Fermi energy is provided by a comparison of the experimental heat capacities with the calculated ones in table 7 in connection with figure 5. The heat capacity γ_{exp} used in table 7 was measured by Heiniger *et al* (1966). In the theoretical coefficients γ_{th} enters only the calculated DOS. So the ratio $\gamma_{exp}/\gamma_{th} = 1 + \lambda$ represents the electron–phonon enhancement λ of γ. The empirical values $1+\lambda_{emp}$ are based on measured thermal properties entering McMillans formula (John 1983). A comparison of $1 + \lambda$ and $1 + \lambda_{emp}$ shows that the calculated DOS are generally too large. If the Fermi energy decreases by only a few mRy with respect to the d bands, it slides into the spin–orbit split energy range of the third band near the point H in the IBZ, and the DOS is appreciably depressed. Because of this distinct experimental indication we computed T_1^{-1} on trial at the energy $E_F - 5$ mRy. In doing so T_1^{-1} falls short of the measured value, and the enhancement of γ by electron–phonon interactions is overestimated. A relative band shift of about 3 mRy explains the experimental T_1^{-1} value. So there is considerable evidence that the spin–orbit splitting is responsible for the large error in Asada and in our Zr relaxation rate.

Table 7. Total DOS $N(E_F)$, temperature coefficient γ of the heat capacity $C = \gamma T$ and relaxation rate $(T_1T)^{-1}$ of Zr.

	Jepsen *et al*	This work $E = E_F$	This work $E = E_F - 5$ mRy	γ_{exp}
$N(E_F)$ (states/atom Ry)	13.1	12.84	8.48	
γ_{th} (mJ mol^{-1} K^{-2})	2.27	2.22	1.47	2.78
$\gamma_{exp}/\gamma_{th} = (1 + \lambda)$	1.22	1.25	1.89	
Emp. enhancement $(1 + \lambda_{emp})$	1.45	1.45	1.45	
$(T_1T)^{-1}$ (sK)$^{-1}$		0.0648	0.0295	
$(T_1T)^{-1}_{exp}$ (sK)$^{-1}$		0.035 ± 0.005		

4.3. Quadrupole scattering

Finally, we point out here some results on nuclear quadrupole relaxation.

This mechanism is brought about by fluctuating field gradients of scattering conduction electrons. As the nuclear spin levels are about seven orders of magnitude lower than electronic energies the electrons scatter quasielastically, and consequently only electrons at the Fermi energy take part. Therefore one difference between the calculation of static gradients of the crystal field and the determination of quadrupolar relaxation is that, in the former case, all band electrons contribute and in the latter case only electrons near the Fermi energy contribute. The estimation of field gradients has a long tradition in the Sternheimer anti-shielding concept (Sternheimer 1950). The anti-shielding theory, mostly applied to insulators, proceeded originally from the assumption that the dominant contribution to the gradient is also induced into the local atomic environment from the surrounding lattice in metals (Watson *et al* 1965). From the present viewpoint it appears to be a more local phenomenon (Kaufman and Vianden 1979) in most metallic systems. The decisive reversal

was initiated by the graphical confrontation of calculated lattice contributions against the (essentially) measured electronic contributions, as given by the difference between the measured value and lattice contribution. Using all available data this revealed the so-called universal correlation (Raghavan *et al* 1975, Raghavan 1976). Crudely stated it proved that, relatively independently of the particular metal, the measured total field gradient is about twice the amount of the calculated non-local lattice contribution, which has opposite sign:

$$q_{zz} = -K(1-\gamma_\infty)q_{zz}^{\text{latt}} \qquad K \approx 2. \tag{18}$$

So the local electronic site contribution is three times that from interatomic Sternheimer polarization, described by the anti-shielding factor γ_∞. Recent full-potential calculations of Blaha *et al* (1988) intensify this fact. According to them, lattice terms contribute only 10–15%, though a direct comparison with anti-shielding calculations is not possible. The local character of the field gradient lends support to the fact that the quadrupole coupling is mainly covered by (10). The quadrupolar spin–lattice relaxation possesses some relationships with the field gradients in HCP metals. The dominance of the p contributions is confirmed for the quadrupole rates in all metals, except for Os. In our calculations the $(p_{1/2} - p_{3/2})$ term contributes dominantly.

Re is the only measured metal in which the quadrupole relaxation is at least comparable with the magnetic relaxation. The good agreement between theory and experiment supports the usability of the calculations of $q_{\kappa\kappa}$. The recovery of the nuclear magnetization in Re shows a multi-exponential behaviour, due to the considerable electrostatic quadrupole splitting of the nuclear levels. The measured T_1 in Re was determined by a fit of the magnetization curve to the theoretical behaviour for pure magnetic relaxation of the $\pm\frac{1}{2}$ transition (in NMR) and the $\pm\frac{1}{2}, \pm\frac{3}{2}$ transition (in NQR) for $I = \frac{5}{2}$. The portion of quadrupole relaxation is, according to table 8, about 20%. As may be seen in table 4, the agreement between theory and experiment is excellent. Lu and Hf possess very strong quadrupole interactions (see for example table 8). Because of the strong quadrupolar line broadening it appears doubtful that NMR/NQR spectra can be obtained in pure metallic Lu and Hf. Os could be suitable for investigating quadrupole relaxation if it allows saturation of the quadrupolar broadened lines. One of the Os isotopes has a spin $I = \frac{3}{2}$. Since the other isotope is purely magnetically relaxed ($I = \frac{1}{2}$), the quadrupole relaxation may be directly extracted. Unfortunately, the latter isotope has a very small natural abundance.

Often the ratio of quadrupole and magnetic spin–lattice relaxation is of interest. Obata (1964) presented an estimation of the ratio between the quadrupole and the magnetic dipolar relaxation rate. Proceeding on the assumption that the nuclear system is relaxed purely either by p or by d electrons, one finds in the spherical case the modified Obata ratio for the total magnetic relaxation

$$\frac{(T_1^{-1})_{\text{q}}^{l}}{(T_1^{-1})_{\text{mag}}^{l}} = 1.82\left(\frac{2I+3}{2I-1}\right)\left(\frac{Q}{\mu}\right)^2 r_l$$

$$r_{\text{p}} = \tfrac{3}{13} \qquad r_{\text{d}} = \tfrac{1}{15} \tag{19}$$

with the nuclear magnetic moment μ in units of nuclear magnetons and Q in barns; $(T_1^{-1})_{\text{mag}}^{l}$ is the sum of the dipole and orbital relaxation rate by states of angular momentum l. Table 8 contains the ratio $(T_1^{-1})_{\text{q}}/(T_1^{-1})_{\text{mag}}$ from the numerical results and the ratios (19) with r_{p} and r_{d}. At the beginning of each period the numerical ratios are close to the ratio (19) using r_{p}, while the results in the middle of the period reflect mainly d relaxation.

Table 8. Nuclear data, ratios between the quadrupolar and magnetic relaxation rate $(T_1^{-1})_q/(T_1^{-1})_{mag}$ using the numerical results, and ratios $(T_1^{-1})_q^l/(T_1^{-1})_{mag}^l$ from (19).

	$\mu(\mu_N)$[a]	Q (barn)[a]	I	$(T_1^{-1})_q/(T_1^{-1})_{mag}$	$(T_1^{-1})_q^p/(T_1^{-1})_{mag}^p$	$(T_1^{-1})_q^d/(T_1^{-1})_{mag}^d$
$^{45}_{21}$Sc	4.7492	−0.22	7/2	0.0013	0.0015	0.00043
$^{47}_{22}$Ti	−0.7870	0.29	5/2	0.056	0.11	0.033
$^{49}_{22}$Ti	−1.1021	0.24	7/2	0.011	0.033	0.0096
$^{89}_{39}$Y	−0.1368	——	1/2	——	——	——
$^{91}_{40}$Zr	−1.298	−0.21[b]	5/2	0.018	0.022	0.0064
$^{99}_{43}$Tc	5.6573	0.3	9/2	0.00062	0.0018	0.00051
$^{175}_{71}$Lu	2.21	5.6	7/2	3.8	4.5	1.3
$^{176}_{71}$Lu	3.15	8.0	7	3.0	3.5	1.
$^{177}_{72}$Hf	0.61	3.0	7/2	13.	16.9	4.9
$^{179}_{72}$Hf	−0.47	3.0	9/2	19.	26.	7.4
$^{185}_{75}$Re	3.1437	2.7	5/2	0.28	0.62	0.18
$^{187}_{75}$Re	3.1760	2.6	5/2	0.25	0.56	0.16
$^{187}_{76}$Os	0.06374	——	1/2	——	——	——
$^{189}_{76}$Os	0.6506	0.8	3/2	0.59	1.9	0.55

[a] Carter *et al* (1977).
[b] Büttgenbach *et al* (1978).

These results could be useful in the case of considerable static quadrupolar interaction in metals and alloys causing a multi-exponential recovery. In this case the ratio of the electronic transition probabilities W_{mag} to W_1 and W_2 (the quadrupolar electronic transition probability for $\Delta m = 1$ and $\Delta m = 2$, respectively) is needed for the full relaxation matrix. Under the assumption $W_1 \approx W_2 = W_q$, which holds quite well in metals, equation (19) provides (apart from a prefactor) the ratio $W_{mag}/W_{1(2)}$ if an appropriate value r between r_p and r_d is chosen. Some values for metals are given in the fifth column in table 8.

5. Conclusions

In conclusion, we have presented explicit formulae for the nuclear spin–lattice relaxation in HCP metals based on Dirac theory and symmetrized spin–orbit functions. We applied them to 3d, 4d and 5d metals using the self-consistent scalar-relativistic and full-relativistic LMTO method. It was shown that the amount of p relaxation increases from the 3d series to the 5d series within one group. This must be considered when applying s–d-band models. Similarly to Asada and Terakura, we found in Zr a relaxation rate that is twice the experimental one. In addition we utilized other electronic structure data to show that there is strong evidence that this deviation is due to spin–orbit splitting near the Fermi energy. The Fermi surface of Ti was discussed in connection with the relaxation rate. In Re we compared the partition of the total relaxation rate into contributions from different angular momenta with an s–d-band-model analysis. The extension of the Obata ratio to the complete magnetic scattering including orbital interaction was used to estimate the amount of quadrupole scattering. The comparison of these estimates with the numerical values show that the computed values tend more to the ratio for pure p relaxation at the beginning of each period, and to the ratio for d scattering in the centre of a period.

Acknowledgments

One of us (RM) is very grateful to Dr H Skriver for use of his LMTO program packages; RM would also like to thank the former Zentralinstitut für Festkörper- und Werkstofforschung, Dresden, for their kind hospitality during his stay there, where he profited by helpful discussions with Professor H Eschrig and Dr M Richter. Thanks are also due to Professor D Brinkmann, Dr M Mali and Dr J Roos for numerous useful discussions.

Appendix. Expressions for the spin–lattice relaxation rate

The relaxation rates are classified with respect to the orbital angular momenta. In our convention the diagonal relaxation rates are designated by one index and the off-diagonal rates are designated by two. The magnetic relaxation rate then contains the following members:

$$\left(\frac{1}{T_1}\right)_{\text{mag}} = \left(\frac{1}{T_1}\right)^{\text{s}}_{\text{mag}} + \left(\frac{1}{T_1}\right)^{\text{p}}_{\text{mag}} + \left(\frac{1}{T_1}\right)^{\text{d}}_{\text{mag}} + \left(\frac{1}{T_1}\right)^{\text{sd}}_{\text{mag}} + \left(\frac{1}{T_1}\right)^{\text{pd}}_{\text{mag}}. \tag{A1}$$

In the following formulae β is the angle between the crystal c axis and the external magnetic field. For the diagonal terms we get

$$C_{\text{M}} = \frac{4\pi k_{\text{B}} T}{\hbar}(\hbar\gamma_{\text{N}})^2 \tag{A2}$$

$$\left(\frac{1}{T_1}\right)^{\text{s}}_{\text{mag}} = C_{\text{M}} H^2_{-1-1} \tfrac{4}{9} (n^{\Gamma_7}_{-1-1})^2 \tag{A3}$$

$$\begin{aligned}\left(\frac{1}{T_1}\right)^{\text{p}}_{\text{mag}} = C_{\text{M}}[\![& H^2_{11} \tfrac{4}{9}(n^{\Gamma_8}_{11})^2 + H^2_{-2-2}\tfrac{8}{225}\{4[2(n^{\Gamma_8}_{-2-2})^2 + 3n^{\Gamma_8}_{-2-2}n^{\Gamma_9}_{-2-2}] \\ & + 3[-(n^{\Gamma_8}_{-2-2})^2 + 3(n^{\Gamma_9}_{-2-2})^2 - 2n^{\Gamma_8}_{-2-2}n^{\Gamma_9}_{-2-2}]\sin^2\beta\} \\ & + H^2_{1-2}\tfrac{1}{18}\{2[n^{\Gamma_8}_{11}n^{\Gamma_8}_{-2-2} + 3n^{\Gamma_8}_{11}n^{\Gamma_9}_{-2-2} + \text{Re}(n^{\Gamma_8}_{1-2})^2] \\ & + 3(n^{\Gamma_8}_{11}n^{\Gamma_8}_{-2-2} - n^{\Gamma_8}_{11}n^{\Gamma_9}_{-2-2} + \text{Re}|n^{\Gamma_8}_{1-2}|^2)\sin^2\beta\} \\ & + H_{11}H_{1-2}\tfrac{2\sqrt{2}}{9}\,\text{Re}[n^{\Gamma_8}_{11}n^{\Gamma_8}_{1-2}(-2+3\sin^2\beta)] \\ & + H_{1-2}H_{-2-2}\tfrac{8\sqrt{2}}{45}\,\text{Re}[-2n^{\Gamma_8}_{1-2}n^{\Gamma_8}_{-2-2} + 3n^{\Gamma_8}_{1-2}n^{\Gamma_9}_{-2-2}(1-\sin^2\beta)] \\ & + H_{11}H_{-2-2}\tfrac{8}{45}|n^{\Gamma_8}_{1-2}|^2(4-3\sin^2\beta)]\!]\end{aligned} \tag{A4}$$

$$\begin{aligned}\left(\frac{1}{T_1}\right)^{\text{d}}_{\text{mag}} = C_{\text{M}}[\![& H^2_{22}\tfrac{8}{225}\{4[2(n^{\Gamma_7}_{22})^2 + 3n^{\Gamma_7}_{22}n^{\Gamma_9}_{22}] \\ & + 3[-(n^{\Gamma_7}_{22})^2 + 3(n^{\Gamma_9}_{22})^2 - 2n^{\Gamma_7}_{22}n^{\Gamma_9}_{22}]\sin^2\beta\} \\ & + H^2_{-3-3}\tfrac{9}{1225}\{4[9(n^{\Gamma_7}_{-3-3})^2 + 10n^{\Gamma_8}_{-3-3}n^{\Gamma_9}_{-3-3} + 16n^{\Gamma_7}_{-3-3}n^{\Gamma_9}_{-3-3}] \\ & + 2[-8(n^{\Gamma_7}_{-3-3})^2 + 25(n^{\Gamma_8}_{-3-3})^2 + 9(n^{\Gamma_9}_{-3-3})^2 \\ & - 16n^{\Gamma_7}_{-3-3}n^{\Gamma_9}_{-3-3} - 10n^{\Gamma_8}_{-3-3}n^{\Gamma_9}_{-3-3}]\sin^2\beta\}\end{aligned}$$

$$
\begin{aligned}
&+ H_{2-3}^2 \tfrac{1}{50}\{2[3n_{22}^{\Gamma_7}n_{-3-3}^{\Gamma_7} + 6n_{22}^{\Gamma_7}n_{-3-3}^{\Gamma_9} + n_{22}^{\Gamma_9}n_{-3-3}^{\Gamma_7} + 10n_{22}^{\Gamma_9}n_{-3-3}^{\Gamma_8} \\
&+ 3\,\mathrm{Re}(n_{2-3}^{\Gamma_7})^2 - 2\sqrt{6}\,\mathrm{Re}(n_{2-3}^{\Gamma_7}n_{2-3}^{\Gamma_9})] \\
&+ [9n_{22}^{\Gamma_7}n_{-3-3}^{\Gamma_7} - 6n_{22}^{\Gamma_7}n_{-3-3}^{\Gamma_9} - n_{22}^{\Gamma_9}n_{-3-3}^{\Gamma_7} - 10n_{22}^{\Gamma_9}n_{-3-3}^{\Gamma_8} \\
&+ 8n_{22}^{\Gamma_9}n_{-3-3}^{\Gamma_9} + 9\,\mathrm{Re}(n_{2-3}^{\Gamma_7})^2 + 2\sqrt{6}\,\mathrm{Re}n_{2-3}^{\Gamma_7}n_{2-3}^{\Gamma_9} + 8\,\mathrm{Re}(n_{2-3}^{\Gamma_9})^2]\sin^2\beta\} \\
&+ H_{22}H_{2-3}\tfrac{4}{75}\,\mathrm{Re}[-4\sqrt{6}n_{22}^{\Gamma_7}n_{2-3}^{\Gamma_7} - 12n_{22}^{\Gamma_7}n_{2-3}^{\Gamma_9} + 2\sqrt{6}n_{22}^{\Gamma_9}n_{2-3}^{\Gamma_7} \\
&+ (4\sqrt{6}n_{22}^{\Gamma_7}n_{2-3}^{\Gamma_7} + 6n_{22}^{\Gamma_7}n_{2-3}^{\Gamma_9} - \sqrt{6}n_{22}^{\Gamma_9}n_{2-3}^{\Gamma_7} + 12n_{22}^{\Gamma_9}n_{2-3}^{\Gamma_9})\sin^2\beta] \\
&+ H_{2-3}H_{-3-3}\tfrac{6}{175}\,\mathrm{Re}[2(-3\sqrt{6}n_{2-3}^{\Gamma_7}n_{-3-3}^{\Gamma_7} + 4\sqrt{6}n_{2-3}^{\Gamma_7}n_{-3-3}^{\Gamma_9} \\
&- 4n_{2-3}^{\Gamma_9}n_{-3-3}^{\Gamma_7} + 10n_{2-3}^{\Gamma_9}n_{-3-3}^{\Gamma_8}) \\
&+ (\sqrt{6}n_{2-3}^{\Gamma_7}n_{-3-3}^{\Gamma_7} - 4\sqrt{6}n_{2-3}^{\Gamma_7}n_{-3-3}^{\Gamma_9} + 4n_{2-3}^{\Gamma_9}n_{-3-3}^{\Gamma_7} - 10n_{2-3}^{\Gamma_9}n_{-3-3}^{\Gamma_8} \\
&- 12n_{2-3}^{\Gamma_9}n_{-3-3}^{\Gamma_9})\sin^2\beta] \\
&+ H_{22}H_{-3-3}\tfrac{8}{175}[4(3|n_{2-3}^{\Gamma_7}|^2 - 2\sqrt{6}\,\mathrm{Re}n_{2-3}^{\Gamma_7}n_{-32}^{\Gamma_9}) \\
&+ (-7|n_{2-3}^{\Gamma_7}|^2 - 9|n_{2-3}^{\Gamma_9}|^2 + 4\sqrt{6}\,\mathrm{Re}n_{2-3}^{\Gamma_7}n_{-32}^{\Gamma_9})\sin^2\beta]]. \qquad \text{(A5)}
\end{aligned}
$$

Re denotes the real part of the mixed DOS product. The non-diagonal contributions arise from terms of the form

$$\langle\Gamma\gamma\kappa_1(l)|H_{mag}|\Gamma'\gamma'\kappa_1'(l)\rangle\langle\Gamma\gamma\kappa_2(l')|H_{mag}|\Gamma'\gamma'\kappa_2'(l')\rangle^* \qquad l \neq l' \qquad \text{(A6)}$$

$$
\begin{aligned}
\left(\frac{1}{T_1}\right)_{\mathrm{mag}}^{\mathrm{sd}} &= C_{\mathrm{M}}[H_{-1-1}H_{2-3}\tfrac{2\sqrt{6}}{15}\,\mathrm{Re}n_{-12}^{\Gamma_7}n_{-1-3}^{\Gamma_7}(-2-3\sin^2\beta) \\
&+ H_{-1-1}H_{22}\tfrac{8}{45}|n_{-12}^{\Gamma_7}|^2(4-3\sin^2\beta) \\
&+ H_{-1-1}H_{-3-3}\tfrac{8}{35}|n_{-1-3}^{\Gamma_7}|^2(3-2\sin^2\beta)] \qquad \text{(A7)}
\end{aligned}
$$

$$
\begin{aligned}
\left(\frac{1}{T_1}\right)_{\mathrm{mag}}^{\mathrm{pd}} &= C_{\mathrm{M}}\{H_{11}H_{-3-3}\tfrac{4}{7}|n_{-31}^{\Gamma_8}|^2\sin^2\beta + H_{1-2}H_{-32}\tfrac{\sqrt{30}}{15}\,\mathrm{Re}n_{-22}^{\Gamma_9}n_{-31}^{\Gamma_8}(-2+\sin^2\beta) \\
&+ H_{1-2}H_{-3-3}\tfrac{2}{35}\,\mathrm{Re}[-2\sqrt{30}n_{-2-3}^{\Gamma_9}n_{-31}^{\Gamma_8} \\
&+ (10\sqrt{2}n_{-2-3}^{\Gamma_8}n_{-31}^{\Gamma_8} + \sqrt{30}n_{-2-3}^{\Gamma_9}n_{-31}^{\Gamma_8})\sin^2\beta] \\
&+ H_{-2-2}H_{22}\tfrac{16}{25}|n_{-22}^{\Gamma_9}|^2\sin^2\beta \\
&+ H_{-2-2}H_{2-3}\tfrac{8}{75}\,\mathrm{Re}[-2\sqrt{15}n_{-2-3}^{\Gamma_8}n_{2-2}^{\Gamma_9} \\
&+ (\sqrt{15}n_{-2-3}^{\Gamma_8}n_{2-2}^{\Gamma_9} + 6n_{-2-3}^{\Gamma_9}n_{2-2}^{\Gamma_9})\sin^2\beta] \\
&+ H_{-2-2}H_{-3-3}\tfrac{8}{175}\,\mathrm{Re}[-4\sqrt{15}n_{-3-2}^{\Gamma_8}n_{-2-3}^{\Gamma_9} \\
&+ (-5|n_{-2-3}^{\Gamma_8}|^2 - 9|n_{-2-3}^{\Gamma_9}|^2 + 2\sqrt{15}n_{-3-2}^{\Gamma_8}n_{-2-3}^{\Gamma_9})\sin^2\beta]\}. \qquad \text{(A8)}
\end{aligned}
$$

We are lead to similar formulae for the quadrupole relaxation:

$$\left(\frac{1}{T_1}\right)_q = \left(\frac{1}{T_1}\right)_q^{\mathrm{p}} + \left(\frac{1}{T_1}\right)_q^{\mathrm{d}} + \left(\frac{1}{T_1}\right)_q^{\mathrm{pd}} \tag{A9}$$

$$C_Q = \frac{4\pi k_B T}{\hbar}\left(\frac{e^2}{4\pi\epsilon_0}Q\right)^2 \tag{A10}$$

$$\begin{aligned}\left(\frac{1}{T_1}\right)_q^{\mathrm{p}} = C_Q[\![& q^2_{-2-2}\tfrac{1}{100}\{20n^{\Gamma_8}_{-2-2}n^{\Gamma_9}_{-2-2} + 3[(n^{\Gamma_8}_{-2-2})^2 + (n^{\Gamma_9}_{-2-2})^2 - 2n^{\Gamma_8}_{-2-2}n^{\Gamma_9}_{-2-2}]\sin^2\beta\} \\ & + q^2_{1-2}\tfrac{1}{100}\{2[3n^{\Gamma_8}_{11}n^{\Gamma_8}_{-2-2} + 17n^{\Gamma_8}_{11}n^{\Gamma_9}_{-2-2} - 3\,\mathrm{Re}(n^{\Gamma_8}_{1-2})^2] \\ & + 3[7n^{\Gamma_8}_{11}n^{\Gamma_8}_{-2-2} - 7n^{\Gamma_8}_{11}n^{\Gamma_9}_{-2-2} + \mathrm{Re}(n^{\Gamma_8}_{1-2})^2]\sin^2\beta\} \\ & + q_{1-2}q_{-2-2}\tfrac{\sqrt{2}}{50}\,\mathrm{Re}[14n^{\Gamma_8}_{1-2}n^{\Gamma_9}_{-2-2} - 3(2n^{\Gamma_8}_{1-2}n^{\Gamma_8}_{-2-2} + 5n^{\Gamma_8}_{1-2}n^{\Gamma_9}_{-2-2})\sin^2\beta]]\end{aligned} \tag{A11}$$

$$\begin{aligned}\left(\frac{1}{T_1}\right)_q^{\mathrm{d}} = C_Q[\![& q^2_{22}\tfrac{1}{100}\{20n^{\Gamma_7}_{22}n^{\Gamma_9}_{22} + 3[(n^{\Gamma_7}_{22})^2 + (n^{\Gamma_9}_{22})^2 - 2n^{\Gamma_7}_{22}n^{\Gamma_9}_{22}]\sin^2\beta\} \\ & + q^2_{-3-3}\tfrac{3}{1225}\{20(2n^{\Gamma_7}_{-3-3}n^{\Gamma_8}_{-3-3} + 4n^{\Gamma_7}_{-3-3}n^{\Gamma_9}_{-3-3} + n^{\Gamma_8}_{-3-3}n^{\Gamma_9}_{-3-3}) \\ & + [16(n^{\Gamma_7}_{-3-3})^2 + 25(n^{\Gamma_8}_{-3-3})^2 + (n^{\Gamma_9}_{-3-3})^2 \\ & - 30n^{\Gamma_7}_{-3-3}n^{\Gamma_8}_{-3-3} - 42n^{\Gamma_7}_{-3-3}n^{\Gamma_9}_{-3-3} + 30n^{\Gamma_8}_{-3-3}n^{\Gamma_9}_{-3-3}]\sin^2\beta\} \\ & + q^2_{2-3}\tfrac{1}{4900}\{10[5n^{\Gamma_7}_{22}n^{\Gamma_7}_{-3-3} + 32n^{\Gamma_7}_{22}n^{\Gamma_8}_{-3-3} + 26n^{\Gamma_7}_{22}n^{\Gamma_9}_{-3-3} \\ & + 15n^{\Gamma_9}_{22}n^{\Gamma_7}_{-3-3} + 6n^{\Gamma_9}_{22}n^{\Gamma_8}_{-3-3} - 5\,\mathrm{Re}(n^{\Gamma_7}_{2-3})^2 + 14\sqrt{6}\,\mathrm{Re}n^{\Gamma_7}_{2-3}n^{\Gamma_9}_{2-3}] \\ & + 3[37n^{\Gamma_7}_{22}n^{\Gamma_7}_{-3-3} - 80n^{\Gamma_7}_{22}n^{\Gamma_8}_{-3-3} - 62n^{\Gamma_7}_{22}n^{\Gamma_9}_{-3-3} \\ & + 3n^{\Gamma_9}_{22}n^{\Gamma_7}_{-3-3} + 30n^{\Gamma_9}_{22}n^{\Gamma_8}_{-3-3} + 72n^{\Gamma_9}_{22}n^{\Gamma_9}_{-3-3} \\ & - 13\,\mathrm{Re}(n^{\Gamma_7}_{2-3})^2 - 26\sqrt{6}\,\mathrm{Re}(n^{\Gamma_7}_{2-3}n^{\Gamma_9}_{2-3}) + 72\,\mathrm{Re}(n^{\Gamma_9}_{2-3})^2]\sin^2\beta\} \\ & + q_{22}q_{2-3}\tfrac{1}{350}\,\mathrm{Re}[10(-6n^{\Gamma_7}_{22}n^{\Gamma_9}_{2-3} - \sqrt{6}n^{\Gamma_9}_{22}n^{\Gamma_7}_{2-3}) \\ & + 3(-2\sqrt{6}n^{\Gamma_7}_{22}n^{\Gamma_7}_{2-3} + 18n^{\Gamma_7}_{22}n^{\Gamma_9}_{2-3} + 7\sqrt{6}n^{\Gamma_9}_{22}n^{\Gamma_7}_{2-3} + 12n^{\Gamma_9}_{22}n^{\Gamma_9}_{2-3})\sin^2\beta] \\ & + q_{2-3}q_{-3-3}\tfrac{2}{1225}\,\mathrm{Re}[10(-4\sqrt{6}n^{\Gamma_7}_{2-3}n^{\Gamma_8}_{-3-3} + 5\sqrt{6}n^{\Gamma_7}_{2-3}n^{\Gamma_9}_{-3-3} \\ & + 9n^{\Gamma_9}_{2-3}n^{\Gamma_7}_{-3-3} - 3n^{\Gamma_9}_{2-3}n^{\Gamma_8}_{-3-3}) \\ & + 3(-4\sqrt{6}n^{\Gamma_7}_{2-3}n^{\Gamma_7}_{-3-3} + 10\sqrt{6}n^{\Gamma_7}_{2-3}n^{\Gamma_8}_{-3-3} - 11\sqrt{6}n^{\Gamma_7}_{2-3}n^{\Gamma_9}_{-3-3} \\ & - 9n^{\Gamma_9}_{2-3}n^{\Gamma_7}_{-3-3} - 15n^{\Gamma_9}_{2-3}n^{\Gamma_8}_{-3-3} - 6n^{\Gamma_9}_{2-3}n^{\Gamma_9}_{-3-3})\sin^2\beta] \\ & + q_{22}q_{-3-3}\tfrac{1}{175}\,\mathrm{Re}[-20\sqrt{6}\,\mathrm{Re}n^{\Gamma_7}_{2-3}n^{\Gamma_9}_{-32} \\ & + 3(4|n^{\Gamma_7}_{2-3}|^2 + \mathrm{Re}\,8\sqrt{6}n^{\Gamma_7}_{2-3}n^{\Gamma_9}_{-32} - |n^{\Gamma_9}_{2-3}|^2)\sin^2\beta]\!].\end{aligned} \tag{A12}$$

The non-diagonal contributions are due to combinations

$$\langle \Gamma\gamma\kappa_1(l)|H_q|\Gamma'\gamma'\kappa_1'(l)\rangle\langle \Gamma\gamma\kappa_2(l')|H_q|\Gamma'\gamma'\kappa_2'(l')\rangle^* \qquad l \neq l' \tag{A13}$$

$$\begin{aligned}\left(\frac{1}{T_1}\right)_q^{pd} = C_Q\{&q_{1-2}q_{2-3}\tfrac{\sqrt{30}}{350}\,\mathrm{Re}[n_{1-3}^{\Gamma_8}n_{-2-2}^{\Gamma_9}(2+3\sin^2\beta)]\\ &+ q_{1-2}q_{-3-3}\tfrac{1}{175}\,\mathrm{Re}[-2\sqrt{30}n_{1-3}^{\Gamma_8}n_{-32}^{\Gamma_9}\\ &+ 3(10\sqrt{2}n_{1-3}^{\Gamma_8}n_{-3-2}^{\Gamma_8} - \sqrt{30}n_{1-3}^{\Gamma_8}n_{-32}^{\Gamma_9})\sin^2\beta]\\ &+ q_{-2-2}q_{22}\tfrac{3}{50}|n_{-22}^{\Gamma_9}|^2\sin^2\beta + q_{-2-2}q_{-32}\tfrac{1}{175}\,\mathrm{Re}[-2\sqrt{30}n_{-2-3}^{\Gamma_8}n_{2-2}^{\Gamma_9}\\ &+ 3(-\sqrt{15}n_{-22}^{\Gamma_9}n_{-3-2}^{\Gamma_8} + 6n_{-22}^{\Gamma_9}n_{-3-2}^{\Gamma_9})\sin^2\beta]\\ &+ q_{-2-2}q_{-3-3}\tfrac{1}{175}\,\mathrm{Re}[4\sqrt{30}n_{-2-3}^{\Gamma_8}n_{-3-2}^{\Gamma_9}\\ &+ 3(-5|n_{-2-3}^{\Gamma_8}|^2 - |n_{-2-3}^{\Gamma_9}|^2 + 2\sqrt{30}\,\mathrm{Re}\,n_{-2-3}^{\Gamma_8}n_{-3-2}^{\Gamma_9})\sin^2\beta]\}.\end{aligned} \tag{A14}$$

Terms containing matrix elements with different angular momenta

$$\langle \Gamma\gamma\kappa(l)|H_{hf}|\Gamma'\gamma'\kappa'(l')\rangle \qquad l \neq l' \tag{A15}$$

are not written here since they are negligible (see section 3).

References

Akai H 1988 *Hyp. Int.* **43** 255

Akai H, Akai M, Blügel S, Drittler B, Ebert H, Terakura K, Zeller R and Dederichs P H 1990 *Prog. Theor. Phys. Suppl.* **101** 11

Andersen O K 1975 *Phys. Rev.* B **12** 3060

Asada T and Terakura K 1982 *J. Phys. F: Met. Phys.* **12** 1387

—— 1983 *J. Phys. F: Met. Phys.* **13** 799

Asada T, Terakura K and Jarlborg T 1981 *J. Phys. F: Met. Phys.* **11** 1847

Blaha P, Schwarz K, Dederichs P H 1988 *Phys. Rev.* B **37** 2792

Büttgenbach S, Dicke R, Gebauer H, Kuhnen R and Träber F 1978 *Z. Phys.* A **286** 125

Carter G C, Bennett L H and Kahan D J 1977 *Prog. Mat. Sci.* **20**

*Dimitropoulos P, Bucher J P, Borsa F and Corti M 1989 *Phys. Rev.* B **39** 7232

Eriksson O 1989 *Acta Universitatis Upsaliensis* **203** Uppsala University

Eschrig H 1988 *Optimized LCAO Method and the Electronic Structure of Extended Systems* (Berlin: Akademie) p 182

Everett P M 1972a *Phys. Rev.* B **6** 3553

—— 1972b *Phys. Rev.* B **6** 3559

Gaspari G D, Shyu W and Das T P 1964 *Phys. Rev.* **134** A852

Hebel L C and Slichter C P 1959 *Phys. Rev.* **113** 1504

Heiniger F, Bucher E and Muller J 1966 *Phys. Kondens. Mater.* **5** 243

Hioki T, Kotani M and Masuda Y 1975 *J. Phys. Soc. Japan* **39** 958

Hodges L, Watson R E and Ehrenreich H 1972 *Phys. Rev.* B **5** 3953

Jepsen O 1975 *Phys. Rev.* B **12** 2899

Jepsen O and Andersen O K 1971 *Solid State Commun.* **9** 1763

Jepsen O, Andersen O K and Mackintosh A R 1975 *Phys. Rev.* B **12** 3084

John W 1983 *Ergebnisse in der Elektronentheorie der Metalle* ed P Ziesche and G Lehmann (Berlin: Akademie) p 396

John W, Nemoshkalenko V V and Antonov V N 1983 *Proc. 13th Symp. Electronic Structure* ed P Ziesche (Dresden) p 236

Kaufmann E N, Vianden R J 1979 *Rev. Mod. Phys.* **51** 161
Koelling D D and Harmon B N 1977 *J. Phys. C: Solid State Phys.* **10** 3107
Korringa J 1950 *Physica* **16** 601
Lehmann G and Taut M 1972 *Phys. Stat. Sol.* **54** 469
Markendorf R 1991 *Thesis* TU Dresden
Narath A 1967 *Phys. Rev.* **162** 320
Obata Y 1963 *J. Phys. Soc. Japan* **18** 1020
—— 1964 *J. Phys. Soc. Japan* **19** 2348
Pyykkö P and Toivonen H 1983 *Acta Academiae Aboensis* B **43** (Abo: Abo Akademi) p 22
Pyykkö P, Pajanne E and Inokuti M 1973 *Int. J. Quantum Chem.* **7** 785
Raghavan R S 1976 *Hyp. Int.* **2** 29
Raghavan R S, Kaufmann E N and Raghavan P 1975 *Phys. Rev. Lett.* **34** 1280
Redfield A G 1957 *IBM J. Res. Dev.* **1** 19
Skriver H L 1984 *The LMTO Method* (Berlin: Springer)
Slichter C P 1990 *Principles of Magnetic Resonance* (Berlin: Springer) p 151
Sternheimer R M 1950 *Phys. Rev.* **80** 102
von Barth U and Hedin L 1972 *J. Phys. C: Solid State Phys.* **5** 1629
Watson R E, Gossard A C and Yafet Y 1965 *Phys. Rev* **140** A365
Wyckoff W G 1974 *Crystal Structures* (New York: Interscience)
Yafet Y and Jaccarino V 1964 *Phys. Rev.* **133** A1630